Sixth International Symposium on Turbulence and Shear Flow Phenomena
Seoul, Korea, 22-24 June 2009

FINE SCALE STRUCTURE AND FRACTAL GEOMETRY OF TURBULENT SCALAR MIXING AT HIGH SCHMIDT NUMBERS

Sachinori Ishimoto, Makoto Sato, Takehiko Seo,
Mamoru Tanahashi, Toshio Miyauchi
Department of Mechanical and Aerospace Engineering,
Tokyo Institute of Technology
2-12-1 Ookayama, Meguro-ku, Tokyo 152-8850, Japan
sishimot@navier.mes.titech.ac.jp, msato@navier.mes.titech.ac.jp,
tseo@navier.mes.titech.ac.jp, mtanahas@mes.titech.ac.jp,
tmiyauch@mes.titech.ac.jp

ABSTRACT

Direct numerical simulations (DNS) of temporally developing turbulent mixing layer with non-reactive and reactive scalar transport up to $Sc = 30.0$ have been conducted to investigate the fractal geometry of scalar surfaces in turbulence. Although contour lines of scalar include small scale wrinkling for high Sc, global pattern is similar to that of moderate Sc cases. Effects of Schmidt number and chemical reaction are discussed by applying fractal analyses based on a box-counting method for scalar surfaces obtained from DNS. For high Sc, two fractal dimensions can be defined. The first fractal can be observed in relatively large scales. The dimension of the first fractal coincides with that of moderate Sc number case in the inertial subrange ($D \approx 2.5$). The second fractal dimension of non-reactive scalar can be defined in small scales and shows larger values (about 2.8), which denotes self-similarity of scalar surfaces smaller than the Kolmogorov length. The second fractal dimension of reactive scalar decreases to 2.65 due to the chemical reaction. The inner cutoff of the second fractal reaches to about 10 times Batchelor length scale for high Sc.

INTRODUCTION

The mixing transition in turbulent free shear flows is very important phenomenon in many engineering applications such as chemical process and combustion. This phenomenon can be observed after the turbulence transition of the flow field and enhances scalar mixing significantly (Konrad, 1974; Dimotakis, 2000). However, detailed mechanism of the mixing transition has not been clarified yet. In our previous studies on fine scale structure of turbulence (Tanahashi et al., 1997; 2001; 2004; 2008; Wang et al., 2007), the existence of universal fine scale structure (coherent fine scale structure), which is independent on Reynolds number and type of flow field, have been revealed. The diameter and the maximum azimuthal velocity of coherent fine scale eddies can be scaled by Kolmogorov length (η) and Kolmogorov velocity (u_k), respectively. Except for near-wall turbulence (Tanahashi et al., 2004), the most expected diameter and maximum azimuthal velocity are 8η and $1.2u_k$. It should be noted that the azimuthal velocity of intense fine scale eddies reaches to $3 \sim 4u'_{rms}$ and are closely related to the intermittency of energy dissipation rate. Since the coherent fine scale structure is a dissipative structure of turbulence and the smallest vortical structure, they would have very important roles on the mixing of heat and mass in turbulence.

In turbulent combustion research, fractal geometry of flame surfaces is very important because the area of flame surface is frequently represented by the ratio of the inner to outer cutoff scale raised to the $2 - D$ power (Gouldin et al., 1989) where D is fractal dimension of the flame surface. The fractal dimension and the inner cutoff of the flame surface has been investigated by many experimental studies (Yoshida et al., 1994; Smallwood et al., 1995; Gülder et al., 2000). However, Gülder et al. (2000) and Gülder and Smallwood (1995) have suggested that the fractal dimension and inner cutoff strongly depend on the measurement and do not agree with expressions proposed by many studies (Peters, 1986; Gouldin, 1987; Gülder, 1990; Poinsot et al., 1990). Therefore, detailed information about the inner cutoff and fractal dimension are necessary to construct the high accuracy turbulent combustion model.

In our previous study (Tanahashi et al., 2007), fractal characteristics of scalar surfaces in turbulent mixing layer have been investigated up to $Re_{\omega,0} = 1900$ for $Sc = 0.6$. Fractal dimension of scalar surfaces in the fully-developed turbulent state is independent to Reynolds number and coincides with the theoretical expectation of Mandelbrot (1975) ($D \approx 2.5$). The inner cutoff is 8 times Kolmogorov length both in the transitional and fully-developed state, and coincides with the most expected diameter of coherent fine scale eddy in turbulence. The mixing transition is characterized by the drastic increase of difference between the outer and inner cutoffs ($Re_\lambda \approx 100$). DNS of reactive scalars show that fractal dimension decreases to $2.40 \sim 2.45$ due to the chemical reaction. The inner cutoff, however, is not affected by the chemical reaction and agrees with that of non-reactive scalars for moderate Sc number.

In this study, direct numerical simulations (DNS) of turbulent mixing layer with non-reactive and reactive scalar transports have been conducted to investigate fractal geometry of scalar surface and relationship between scalar mixing and fine scale structure in turbulence for high Sc number.

DIRECT NUMERICAL SIMULATION OF TURBULENT MIXING LAYER

DNS of temporally developing turbulent mixing layer with different Sc were conducted by solving following continuity equation, incompressible Navier-Stokes equations and mass conservation equations;

$$\nabla \cdot \boldsymbol{u} = 0, \tag{1}$$

$$\frac{\partial \boldsymbol{u}}{\partial t} + \boldsymbol{\omega} \times \boldsymbol{u} = -\nabla P + \frac{1}{Re_{\omega,0}} \nabla^2 \boldsymbol{u}, \tag{2}$$

$$\frac{\partial Y_A}{\partial t} + \boldsymbol{u} \cdot \nabla Y_A = \frac{1}{ReSc} \nabla^2 Y_A - RcY_A Y_B, \tag{3}$$

Figure 1: Distributions of scalar mass fraction in fully-developed turbulent state ($t = 150$) for $Re_{\omega,0} = 500$. (a):$Rc = 0$, $Sc = 0.6$, (b):$Rc = 0$, $Sc = 30.0$ and (c):$Rc = 1$, $Sc = 30.0$.

Table 1: Numerical parameters for DNS of temporally-developing turbulent mixing layer with non-reactive and reactive passive scalar($Re_{\omega,0} = 500$).

Run ID	Rc	Sc	$N_x \times N_y \times N_z$
TMLPS1	0	0.6	$216 \times 325 \times 144$
TMLPSH1	0	3.0	$480 \times 721 \times 320$
TMLPSH2	0	6.0	$480 \times 721 \times 320$
TMLPSH3	0	30.0	$1152 \times 1729 \times 768$
TMLRS1	1	0.6	$216 \times 325 \times 144$
TMLRSH1	1	3.0	$480 \times 721 \times 320$
TMLRSH2	1	6.0	$480 \times 721 \times 320$
TMLRSH3	1	30.0	$1152 \times 1729 \times 768$

$$\frac{\partial Y_B}{\partial t} + \boldsymbol{u} \cdot \nabla Y_B = \frac{1}{ReSc}\nabla^2 Y_B - RcY_A Y_B, \qquad (4)$$

where $\boldsymbol{u}$, $\boldsymbol{\omega}$, P and Y_i denote velocity vector, vorticity vector, total pressure ($P = p + \boldsymbol{u}\boldsymbol{u}/2$) and mass fraction of species i, respectively. These equations are non-dimensionalized by a mean velocity difference (ΔU), an initial vorticity thickness ($\delta_{\omega,0} = \Delta U/(\partial\bar{u}/\partial y)_{max}$) and mass concentration in the free stream ($Y_{i,0}$). Dimensionless groups in above equations are Reynolds number ($Re_{\omega,0}$), Schmidt number (Sc) and non-dimensional reaction rate (Rc).

The initial mean velocity distribution was given by a hyperbolic tangent velocity profile: $u(y) = 0.5\tanh(2y)$. Three dimensional random perturbation which has the same turbulent intensity profile with the experimental results (Wygnanski and Fielder, 1970) and banded white noise $|k_i| < 21$ was superposed on the mean velocity (Tanahashi et al., 2001). As for the initial concentration profile of passive scalars are also assumed to be hyperbolic tangent one; $Y_A(y) = 0.5 + 0.5\tanh(2y)$, $Y_B(y) = 0.5 - 0.5\tanh(2y)$. Computational domain was selected to be $4\Lambda \times 6\Lambda \times 8/3\Lambda$, where Λ is the most unstable wave length for the initial mean velocity profile.

All variables are expanded by Fourier series in streamwise (x) and spanwise (z) directions and by sine/cosine series in transverse (y) direction. The boundary condition is periodic in the streamwise and spanwise directions and free-slip in the transverse direction. In the spanwise direction, the size of the computational domain is selected due to the 3/2 instability of the two-dimensional roller (Pierrehumbert and Widnall, 1982). In the transverse direction, that is selected to be enough to avoid mirror vortex effects caused by the free slip boundary condition.

DNS were conducted for $Re_{\omega,0} = 500$ and Schmidt number is changed for $Sc = 0.6$, 3.0, 6.0 and 30.0. To investigate effects of chemical reaction, DNS are conducted for $Rc = 0$ and 1 for each cases by assuming a single step reaction: A + B = 2P. Table 1 shows numerical parameters of the present DNS. The largest DNS are performed in $1152 \times 1729 \times 768$ grid points. Aliasing errors from nonlinear terms in the governing equations are fully removed by 3/2 rule and time integration is conducted by the low-storage version of 3rd order Runge-Kutta scheme. Computations were carried out until after the saturation of the subharmonic mode ($t = 150$) for all cases.

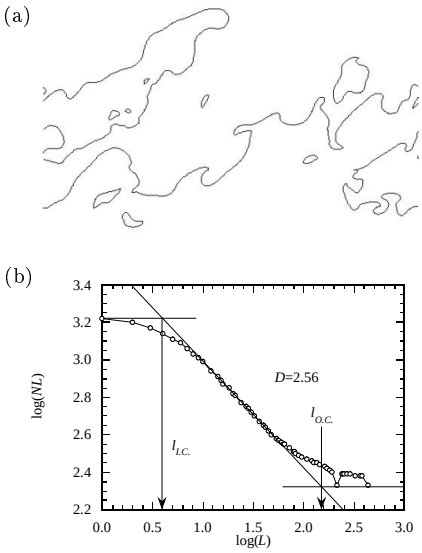

Figure 2: Contour lines of mass fraction (Y=0.5) on a typical $x-y$ plane (a) and $NL-L$ plots for 0.5 contour line of passive scalar on $x-y$ plane (b) for Sc=0.6.

FRACTAL GEOMETRY OF SCALAR SURFACES

Fractal analyses

Figure 1 shows distributions of mass fraction on a $x-y$ plane in fully-developed turbulent state ($t = 150$) for several representative cases. With the increase of Sc, scalar distribution tends to include small scale fluctuation obliviously. For high Sc number reactive case, the scalar distribution becomes more complex, suggesting visualization is not enough to investigate characteristics of scalar mixing. In this study, fractal analyses are introduced similar to our previous study (Tanahashi et al., 2007). As for contour lines on two dimensional cross sections or contour surfaces of scalar, a two-dimensional (2D) or three-dimensional (3D) box counting methods are applied. In the 2D box counting method, contour lines on each $x-y$ or $y-z$ plane such as in Fig. 2(a) are analyzed, and one fractal plot ($NL-L$ plot) is obtained by averaging counting results on all planes as shown in Fig. 2(b). Here, L is the measure and NL is length of contour lines. From the $NL-L$ plot, an inner cutoff ($l_{I.C.}$)

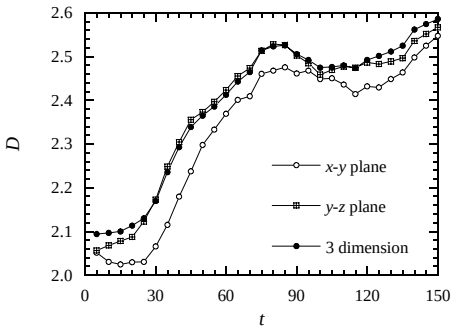

Figure 3: Comparison of fractal dimensions fom two-dimensional cross-section and three-demensional surfaces for Sc=0.6 and Rc=0.

and an outer cutoff ($l_{O.C.}$) can be defined. From a slope of the $NL-L$ plot, fractal dimension (D) is estimated using an additive law. As a result, inner cutoff, outer cutoff and fractal dimension are determined at a given time. As for the 3D box counting method, a fractal plot is obtained directly. The accuracy of the box counting method has been shown by our previous study (Miyauchi et al., 1994).

In Fig. 3, fractal dimensions obtained from two-dimensional cross-section and three-dimensional surfaces are compared for Sc = 0.6. Fractal dimensions increase between t = 30 and t = 80. In this period, the turbulence transition of flow field occurs and lots of coherent fine scale structures are created (Tanahashi et al., 2001). In our previous study (Tanahashi et al., 2007), fractal characteristics of scalar surfaces have been investigated up to $Re_{\omega,0}$ = 1900 for moderate Sc number. In the fully-developed turbulent state (t > 80), the directional dependence of the fractal dimension decreases. Fractal dimension from 3D surfaces coincides with that from $y-z$ planes in the transitional stage, and with that from $x-y$ planes in the fully-developed state. The fractal dimension obtained in our previous DNS of non-reactive scalar is 2.50 which coincides with the theoretical expectation of Mandelbrot (1975). Note that the chemical reaction reduces the fractal dimension to 2.40 $\sim$ 2.45 (Tanahashi et al., 2007).

Effects of Schmidt number

As for turbulent flows with transport of passive scalar with high Sc number, it is well-known that Batchelor length scale (η_B) becomes smaller than Kolmogorov length significantly because it is expressed by $\eta_B = \eta/Sc^{1/2}$. Contour lines of passive scalar (Y_A=0.5) on a $x-y$ plane are shown for different Sc cases in Fig. 4. Distribution of mass fraction becomes more complex for high Sc. Contour lines of scalar include small scale wrinkling for high Sc. It should be noted that global pattern is similar even for different Sc because the turbulence structure is exactly same for these cases. The complexity of the contour lines is caused by local engulfment of scalar due to fine scale motion of turbulence. Figure 5 shows fractal plots ($NL-L$ plots) for Sc = 0.6 and Sc = 30.0. As shown in Fig. 2, only one fractal dimension (D) can be defined for moderate Sc (Tanahashi et al., 2007), which represents the inertial subrange of turbulent velocity fluctuation and self-affinity of scalar surfaces. On the other hand, for high Sc number cases, two fractal dimensions (D_1 and D_2 in Fig. 5) can be defined. The first fractal dimension D_1 can be observed in relatively large scales and coincides with that of moderate Sc number case (D). Furthermore, D_1 nearly coincides for high Sc number cases. The second fractal dimension D_2 can be defined in small scales and shows larger values up to 2.8 and denotes self-similarity of scalar surfaces. Temporal developments of these fractal dimensions are shown in Fig. 6. The first fractal dimension is always small and the second one does large. However, difference between Sc = 6.0 and Sc = 30.0 is not significant. This result suggests that an asymptotic fractal dimension may exist for higher Sc.

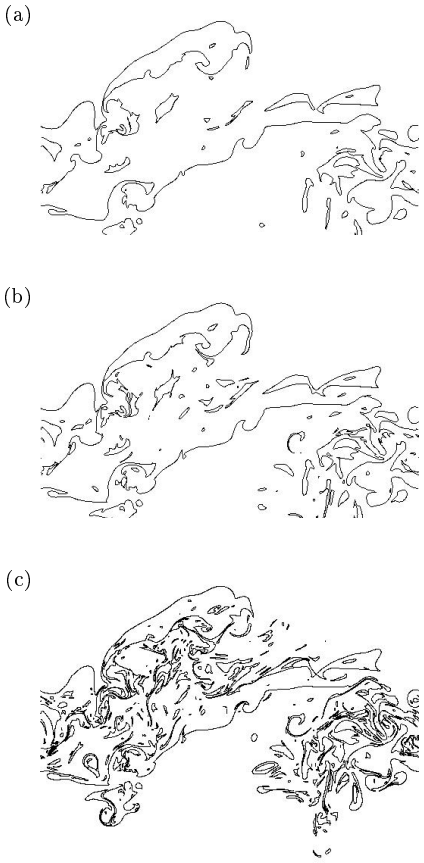

Figure 4: Contour lines of passive scalar (Y_A=0.5) on a typical $x-y$ planes (Rc = 0). (a):Sc = 3.0, (b):Sc = 6.0 and (c):Sc = 30.0.

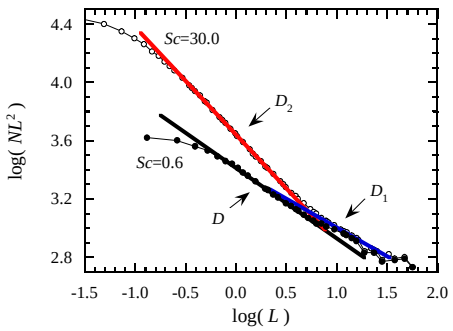

Figure 5: $NL-L$ plots for Sc = 0.6 and Sc = 30.0 (Rc = 0).

In Table 2, inner cutoff of the second fractal is compared with dissipation length scales of velocity and scalar fluctuations in the fully-developed state. Temporal developments of these relations are shown in Fig. 7. The inner cutoff of the second fractal would be scaled by the Batchelor length scale and reaches to about $10\eta_B$. The self-similar fractal in small scales is induced by fine scale stirring of scalar by the coherent fine scale eddy of turbulence. The observation that

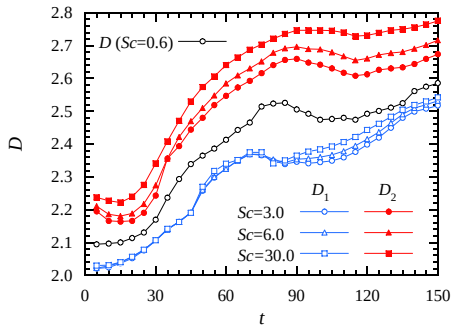

Figure 6: Development of fractal dimension of non-reactive passive scalar with different Sc ($Rc = 0$).

Table 2: Inner cutoff of the second fractal and its relation to dissipation length scales of velocity and non-reactive scalar fluctuations in fully-developed state

Sc	η	η_B	η_B/η	$l_{I.C.}/\eta_B$
0.6	0.0577	0.0745	1.29	6.2958
3.0	0.0577	0.0333	0.58	7.4119
6.0	0.0577	0.0235	0.41	8.4105
30.0	0.0577	0.0105	0.18	9.9436

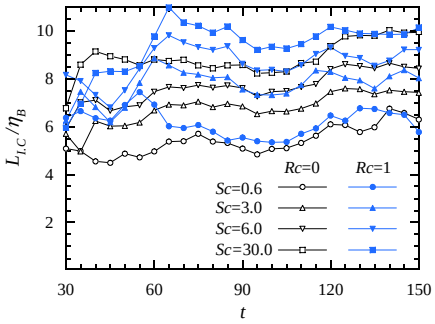

Figure 7: Development of relation of inner cutoff of the second fractal to dissipation length scales of scalar fluctuations.

the contour lines for $Sc = 30.0$ is more complex than that for $Sc = 0.6$ is mainly caused by the scale separation between η and η_B.

In Fig. 5, D_1 and D_2 fractals crossover at a medium scale. In this study, this length scale is defined as a crossover scale ($l_{C.O.}$). Figure 8 shows temporal development of the crossover scale. Here, L_E represents integral length scale of turbulent velocity fluctuation. The crossover scale becomes smaller with the increase of Sc, whereas that is about L_E.

Effects of chemical reaction

Experimental observations in turbulent reactive flows (Gülder and Smallwood, 1995; Gülder et al., 2000) have suggested that fractal dimension of surfaces with chemical reaction such as flame is smaller than that of non-reactive surfaces (Sreenivasan et al., 1989; 1991). In our previous study (Tanahashi et al., 2007), effects of chemical reaction on the fractal geometry have been investigated for the moderate Sc number. The fractal dimension decreases from 2.50 for non-reactive scalar and approaches to 2.40 $\sim$ 2.45 for high reaction rate.

Figure 6 shows contour lines of mass fraction ($Y_A = 0.5$) for reactive cases in the fully-developed turbulent state. As for the reactive cases, distribution of mass fraction depend on Rc for small Rc (Tanahashi et al., 2007). However, for large Rc, distribution of mass fraction scarcely depend on Rc

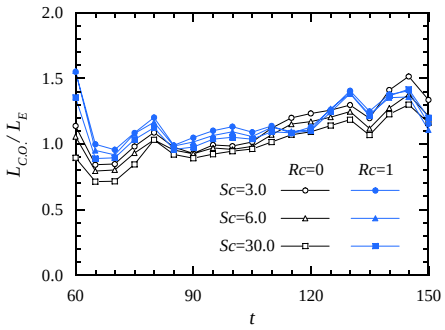

Figure 8: Developments of the crossover scale of D_1 and D_2 fractals.

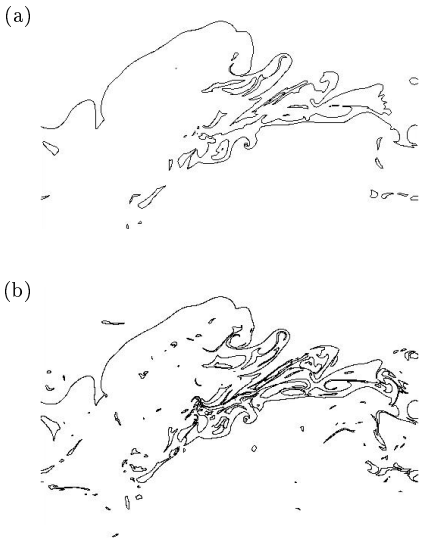

Figure 9: Contour lines of passive scalar (Y_A=0.5) on a typical $x-y$ planes ($Rc = 1$). (a):$Sc = 6.0$ and (b):$Sc = 30.0$.

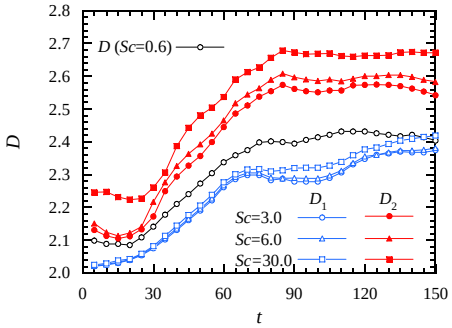

Figure 10: Development of fractal dimension of reactive passive scalar with different Sc ($Rc = 1$).

because the reaction is limited by the turbulent mixing. In Fig. 10, fractal dimension obtained by the 3D box counting method is shown for reactive cases. The first fractal dimension also decreases for high Sc number case compared with non-reactive cases shown in Fig. 6. Similar to the moderate Sc cases, however, the decreasing rate of the fractal dimension is relatively small and D_1 becomes about 2.4. For the second fractal dimension, chemical reaction also reduces surface complexity with about 0.1 dimension. The second fractal dimension of the highest Sc case is about 2.65. The Sc number dependence of this dimension is similar to that of non-reactive cases. In Figs. 7 and 8, temporal developments

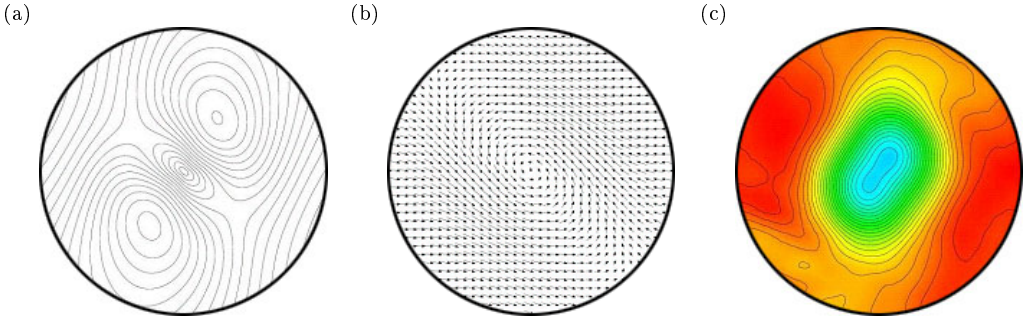

Figure 11: Elliptic feature of the coherent fine scale eddies on the rotating plane. (a):Contour plot of azimuthal velocity, (b):velocity vector and (c):distributions of energy dissipation rate.

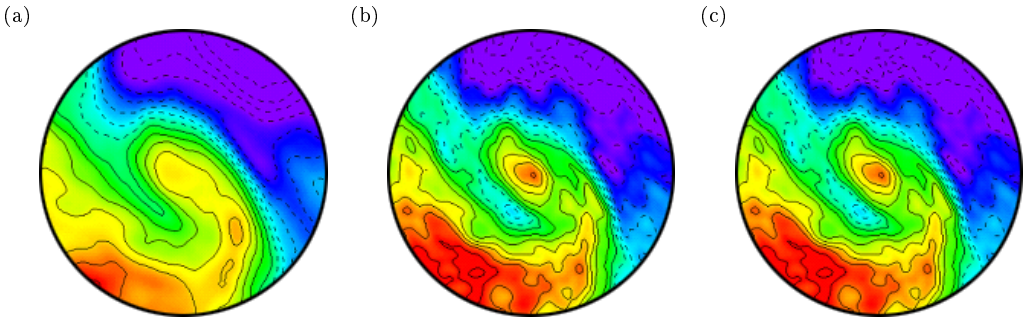

Figure 12: Phase-averaged distributions of scalar mass fraction for (a):$Sc = 0.6$, (b):$Sc = 6.0$ and (c):$Sc = 30.0$ on the plane perpendicular to axis of coherent fine scale eddy.

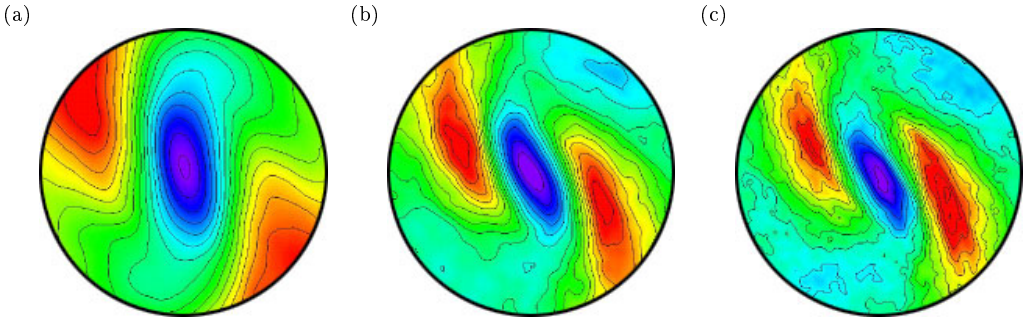

Figure 13: Phase-averaged distributions of scalar dissipation rate for (a):$Sc = 0.6$, (b):$Sc = 6.0$ and (c):$Sc = 30.0$ on the plane perpendicular to axis of coherent fine scale eddy.

of the inner cut off and the crossover scale are also shown for the reactive case. Although the fractal dimension is affected by the chemical reaction, these scales show similar behaviors with non-reactive cases.

MICRO-SCALE SCALAR TRANSPORT

To discuss scalar mixing in small scale, it is important to shows the characteristics of the fine scale eddies. As shown by our previous study on the inner structure of fine scale eddies (Kang et al., 2006), the cross section of the coherent fine scale eddy shows distinct elliptic feature. The azimuthal velocity near the center is dominated by the $k_\theta = 2$ mode, where $k_\theta = 2$ represents azimtuhal wave number. In this study, phase-average is conducted based on the $k_\theta = 2$ mode of the azimuthal velocity. Figure 11 shows contour plots of phase-averaged azimuthal velocity, velocity vectors and distribution of energy dissipation rate. The radius of displayed region in Fig. 11 is $2.0r_c$, where r_c represents radians of the fine scale eddy. Near the center of the fine scale eddy, elliptic feature can be observed in the distribution of the phase-averaged azimuthal velocity. The distribution of radial velocity, which is not shown here, shows existence of distinct inflow into the center and outflow from the center. The velocity vectors constructed from the azimuthal and radial velocity component also shows the asymmetric feature of the fine scale eddy. These feature of the coherent fine scale eddies have been confirmed by PIV measurements (Tanahashi et al., 2002; 2008). The energy dissipation rate shows two minima near the center on the minor axis of the azimuthal velocity distribution and two maxima on major axis.

Scalar distribution around the coherent fine scale eddies are dominated by $k_\theta = 1$, which is different from that of the azimuthal velocity. However, there are strong relation in phase between these dominant modes. Figure 12 shows mean scalar distributions around the eddy. Here, scalar distributions are phase-averaged based on the $k_\theta = 2$ mode of the azimuthal velocity. Due to the elliptic feature of the eddy, the scalar is convoluted towards the center of the eddy and shows the maximum and minimum on the major axis in that plane. Although all cases shows a similar global scalar distributions around the coherent fine scale eddy, engulfments of scalar are enhanced for higher Sc case. In Fig. 13, phase-averaged scalar dissipation rates are shown for three cases. The scalar dissipation rate is also phase-averaged

based on the $k_\theta = 2$ mode of the azimuthal velocity. The scalar dissipation rate shows the maximum and minimum on that plane and their peak values tend to increase and to approach to the center for high Sc case. Furthermore, the locations of the maximum coincide with that of the maximum energy dissipation rate of velocity fluctuation, which suggests analogy between turbulence and scalar fluctuation transport in small scales.

CONCLUSIONS

In this study, direct numerical simulations of turbulent mixing layer with non-reactive and reactive scalar transports have been conducted to investigate turbulent mixing of high Sc number passive scalar.

For high Sc, two fractal dimensions can be defined. The first fractal dimension coincides with that of moderate Sc, whereas the second one shows larger values around 2.8. The inner cutoff of the second fractal reaches to about 10 times of Batchelor length scale for high Sc. DNS of reactive scalars show that the first fractal dimension decreases to $2.40 \sim 2.45$ and the second one does 2.7 due to the chemical reaction. The fact that the inner cutoff for the reactive cases coincides with that of non-reactive cases shows that the coherent fine scale structure of turbulence dominates the mixing and reaction in small scales.

ACKNOWLEDGEMENT

This work is partially supported by Grant-in-Aid for Scientific Research (S)(No. 18106004) of Japan Society for the Promotion of Science.

REFERENCES

Dimotakis, P., 2000, "The Mixing Transition in Turbulent Flows", *Journal of Fluid Mechanics*, Vol. 409, pp. 69-98.

Gouldin, F. C., Bray, K. N. C., and Chen, J. -Y., 1989, "Chemical Closure Model for Fractal Flamelets", *Combustion and Flame*, Vol. 77, pp. 241-259.

Gouldin, F. C., 1987, "An Application of Fractals to Modeling Premixed Turbulent Flames", *Combustion and Flame*, Vol. 68, pp. 249-266.

Gülder, Ö. L., 1990, "Turbulent Premixed Combustion Modelling Using Fractal Geometry", *Proceedings of Combustion Institute*, Vol. 23, pp. 835-842.

Gülder, Ö. L., Smallwood, G. J., 1995, "Inner Cutoff Scale of Flame Surface Wrinkling in Turbulent Premixed Flames ", *Combustion and Flame*, Vol. 103, pp. 107-114.

Gülder, Ö. L., Smallwood, G. J., Wong, R., Snelling, D. R., Smith, R., Deschamps, B. M., and Sautet, J. -C., 2000, "Flame Front Surface Characteristics in Turbulent Premixed Propane/Air Combustion", *Combustion and Flame*, Vol. 120, pp. 407-416.

Konrad, J. H., 1974, "An Experimental Investigation of Mixing in Two-Dimensional Turbulent Shear Flow with Applications to Diffusion-Limited Chemical Reactions", International Report, CIT-8-PU, Calif. Inst. Technol. Pasadena, CA.

Mandelbrot, B. B., 1975, "On the Geometry of Homogeneous Turbulence, with Stress on the Fractal Dimension of the Iso-Surfaces of Scalars", *Journal of Fluid Mechanics*, Vol. 72, pp. 401-416.

Miyauchi, T., Tanahashi M., and Gao, F., 1994, "Fractal Characteristics of Turbulent Diffusion Flames", *Combustion Science and Technology*, Vol. 96, pp. 135-154.

Kang, S. J., Tanahashi, M., and Miyauchi, T., 2006, "Elliptic feature of coherent fine scale eddies in turbulent channel flows", *Journal of Mechanical Science and Technology*, Vol. 20-2, pp. 262-270.

Peters, N., 1986, "Laminar Flamelet Concepts in Turbulent Combustion ", *Proceedings of Combustion Institute*, Vol. 21 pp. 1231-1250.

Pierrehumbert, R. T., and Widnall, S. E., 1982, "The Two- and Three- Dimensional Instabilities of a Spatially Periodic Shear Layer", *Journal of Fluid Mechanics*, Vol. 114, pp. 59-82.

Poinsot, T., Veynante, D., and Candel, S., 1990, "Diagrams of Premixed Turbulent Combustion Based on Direct Simulation", *Proceedings of Combustion Institute*, Vol. 23 pp. 613-619.

Smallwood, G. J., Gülder, Ö. L., Snelling, D. R., Deschamps, B. M., and Gökalp, I., 1995, "Characterization of Flame Front Surfaces in Turbulent Premixed Methane/Air Combustion", *Combustion and Flame*, Vol. 101, pp. 461-470.

Sreenivasan, K. R., Ramshankar, R., and Meneveau, C., 1989, "Mixing, Entrainment and Fractal Dimension of Surfaces in Turbulent Flows", *Proceedings of the Royal Society of London. Series A, Mathematical and Physical Sciences*, Vol. 421, pp. 79-108.

Sreenivasan, K. R., 1991, "Fractals and Multifractals in Fluid Turbulence", *Annual Review of Fluid Mechanics*, Vol. 23, pp. 539-600.

Tanahashi, M., Miyauchi, T., and Ikeda, J., 1997, "Identification of Coherent Fine Scale Structure in Turbulence", *Proceedings of the IUTAM Symposium. Simulation and Identification of Organized Structures in Flows*, pp. 131-140.

Tanahashi, M., Iwase, S., and Miyauchi, T., 2001, "Appearance and Alignment with Strain Rate of Coherent Fine Scale Eddies in Turbulent Mixing Layer", *Journal of Turbulence*, Vol. 2, p. 6.

Tanahashi, M., Ootsu, M., Fukushima, M., and Miyauchi, T., 2002, "Measurement of Coherent Fine Scale Eddies in Turbulent Mixing Layer by DPIV", *Engineering Turbulence Modeling and Measurements*, Vol. 5 p. 525.

Tanahashi, M., Kang, S.-J., Miyamoto, T., Shiokawa, S., and Miyauchi, T., 2004, "Scaling Law of Fine Scale Eddies in Turbulent Channel Flows up to $Re_\tau = 800$", *International Journal of Heat and Fluid Flow*, Vol. 25, pp. 331-340.

Tanahashi, M., Wang, Y., Fujisawa, T., Chinda, K., Sato, M., and Miyauchi, T., 2007, "Fractal Geometry and Mixing Transition in Turbulent Mixing Layer", *Proc. 5th Int. Symp. Turbulence and Shear Flow Phenomena*, Vol. 3, pp. 1187-1192.

Tanahashi, M., Hirayama, T., Taka, S., and Miyauchi, T., 2008, "Measurement of fine scale structure in turbulence by time-resolved dual-plane stereoscopic PIV", *International Journal of Heat and Fluid Flow*, Vol. 29, pp. 792-802.

Yoshida, A., Kasahara, M., Tsuji, H., and Yanagisawa, T., 1994, "Fractal geometry application in estimation of turbulent burning velocity of wrinkled laminar flame", *Combustion Science and Technology*, Vol. 103, pp. 207-218.

Wang, Y., Tanahashi, M., and Miyauchi, T., 2007, "Coherent fine scale eddies in turbulence transition of spatially-developing mixing layer", *International Journal of Heat and Fluid Flow*, Vol. 28, pp. 1280-1290.

Wygnanski, I., and Fielder, H. E., 1970, "The Two-Dimensional Mixing Region", *Journal of Fluid Mechanics*, Vol. 41, pp. 327-361.